Research Article | Vol. 11, No. 10 / 1 Oct 2021 / Optical Materials Express 3567
Optical Materials EXPRESS

Spatially dense integration of micron-scale devices from multiple materials on a single chip via transfer-printing

DIMITARS JEVTICS,[1,5,*] JACK A. SMITH,[1,5] JOHN MCPHILLIMY,[1] BENOIT GUILHABERT,[1] PAUL HILL,[1] CHARALAMBOS KLITIS,[2] ANTONIO HURTADO,[1] MARC SOREL,[2,3] HARK HOE TAN,[4] CHENNUPATI JAGADISH,[4] MARTIN D. DAWSON,[1] AND MICHAEL J. STRAIN[1]

[1]*Institute of Photonics, Department of Physics, University of Strathclyde, Glasgow G1 1RD, UK*
[2]*School of Engineering, University of Glasgow, Glasgow G12 8QQ, UK*
[3]*Institute of Technologies for Communication, Information and Perception (TeCIP), Sant'Anna School of Advanced Studies, Via Moruzzi 1, 56127 Pisa, Italy*
[4]*Department of Electronic Materials Engineering, Research School of Physics, The Australian National University, Canberra, ACT 0200, Australia*
[5]*Authors contributed equally*
[*]*dimitars.jevtics@strath.ac.uk*

Abstract: The heterogeneous integration of devices from multiple material platforms onto a single chip is demonstrated using a transfer-printing (TP) technique. Serial printing of devices in spatially dense arrangements requires that subsequent processes do not disturb previously printed components, even in the case where the print head is in contact with those devices. In this manuscript we show the deterministic integration of components within a footprint of the order of the device size, including AlGaAs, diamond and GaN waveguide resonators integrated onto a single chip. Serial integration of semiconductor nanowire (NW) using GaAs/AlGaAs and InP lasers is also demonstrated with device to device spacing in the 1 μm range.

1. Introduction

Photonic integrated circuit (PIC) technologies have matured from research devices to accessible foundry technologies over the last couple of decades [1–3], enabling their application in fields including telecommunications, optical signal processing and sensing [4]. Initially PIC technologies were fabricated in single material platforms, for example silicon [5] or III-V materials [6], with some flexibility available through deposition of secondary materials such as SiN [7] or regrowth of compound semiconductors [8]. Nevertheless, it is clear that in order to produce future PIC systems, multiple materials are required to be integrated on a single chip to provide for the multiple optical and opto-electronic functions that cannot be optimally realized in a single monolithic platform. The development of hybrid optical platforms has been advanced in recent years driven by telecommunications [9] and quantum photonic applications [10,11]. The most mature of these technologies is integration of III-V materials with silicon PICs, providing optical sources, gain and detectors on the passive silicon platform. Typically, wafers of III-V material can be bonded onto the pre-fabricated silicon devices and then post-processed to form the active optical components [12].

Additionally, the direct growth of III-V on silicon has been demonstrated as a route towards multi-material systems [13–16], where this is typically limited in terms of integration with wafer

#432751 https://doi.org/10.1364/OME.432751
Journal © 2021 Received 16 Jun 2021; revised 7 Aug 2021; accepted 8 Aug 2021; published 29 Sep 2021

Optical Materials EXPRESS

scale pre-fabricated silicon PICs. These methods have posed a significant challenge if more than one additional material is required on the host PIC. This would then require a complex fabrication process of multiple bond and post-bond lithography, etching and deposition steps, whilst previous hybrid devices were in situ.

Alternatively, a pick and place integration process, generally referred to as transfer printing, for thin film devices has been developed to allow local hybrid materials integration on host PICs [17–21]. This can be complemented by post-printing fabrication processes [22] or fully fabricated devices can be transferred [23]. This method provides the freedom to carry out multiple printing processes on a single chip, though most demonstrations to date have focused on the integration of one additional material onto the host PIC. The method relies on the transfer of membrane devices or coupons of material with dimensions in the 1 - 10^3 μm range, and thickness from hundreds of nanometers to a few μm. These membranes are detached from their native substrate using a soft polymer stamp, followed by deposition onto the receiver substrate. This is shown schematically in Fig. 1. One outstanding challenge for this technology is the dense integration of multiple different material devices in a compact footprint to allow for efficient use of chip space and incorporate a range of functions in a single chip. Transfer printing involves the direct contact of the stamp with the receiver when devices are printed, and therefore in processes with multiple printing steps, closely spaced devices will interact with the stamp material, with the potential for removal or shift in position of the device.

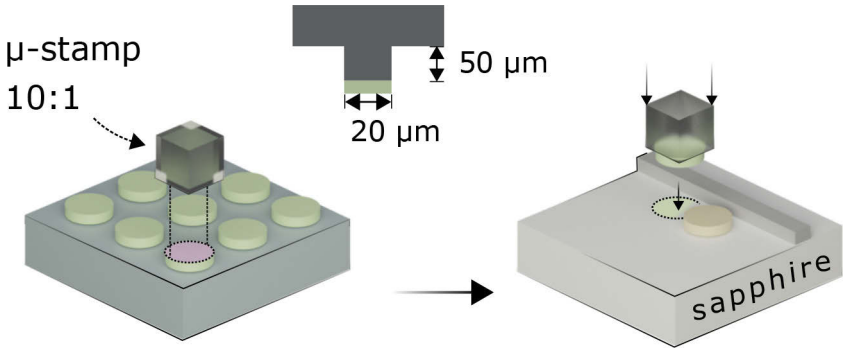

Fig. 1. (a) The transfer-printing process of μ-disk resonators from their original substrate onto a host waveguide structure. The inset shows the cross sectional geometry of the PDMS stamp head. A micro-pillar extends from the main PDMS bulk with a height large enough to allow contact with only one device at a time.

In this work we present a transfer printing process that allows the dense integration of multiple devices, from different material platforms, within a chip footprint that is comparable to the device size. This demonstration is shown for devices with two characteristic length scales, μ-disk resonators with diameters in the few μm range, and NW lasers, with cross-sectional diameters of a few hundred nanometers and major axis length of a few μm. A technique is presented that allows the serial printing of devices with spacings down to the micrometer range. Optical measurements of waveguide coupled resonators and optically pumped NW lasers are presented.

2. Methods

Two demonstrations of dense device integration using transfer printing are presented. Both use the same basic transfer printing toolset as detailed in previous works [17,24,25]. As detailed in the references, the printing process can take less than 1 minute for a single transfer and can be implemented as a parallel transfer process with high yield and accuracy. The device dimensions in each case require tailored processes to allow the close printing of devices.

Optical Materials EXPRESS

2.1. Micro-disk resonators

The first demonstration is the integration of μ-disk resonators in AlGaAs and diamond materials with a GaN-on-sapphire waveguide platform. The diamond, AlGaAs and GaN waveguide devices were all fabricated individually and subsequently integrated using the transfer print method detailed below. All three chips were patterned with electron beam lithography into a hydrogen silsequioxane (HSQ) resist. The device masks were then transferred into the waveguide materials using inductively coupled reactive ion etching (ICP-RIE).

The single crystal diamond material was pre-thinned using an Ar/Cl_2 ICP-RIE stage to around 1.8 μm in thickness [26]. The μ-disk resonator devices were then etched into the diamond using an Ar/O_2 ICP-RIE process. The disk used in the subsequent printing stage had a diameter of 25 μm.

The AlGaAs μ-disk devices were fabricated from a two-layer $Al_{0.2}Ga_{0.8}As$ (270 nm) core on $Al_{0.7}Ga_{0.3}As$ (500 nm) undercladding epitaxial stack on a GaAs substrate [27]. The disk pattern in the HSQ resist was etched down to the substrate using a $SiCl_4/Ar/N_2$ chemistry. This was followed by a buffered HF under-etch of the sacrificial low index $Al_{0.7}Ga_{0.3}As$ layer to release the disks onto the GaAs substrate. Two disks of 10 and 20 μm diameter, respectively, were used in the printing demonstrations.

The GaN-on-sapphire PIC was etched using an Ar/Cl_2 chemistry, before a buffered HF etch was used to remove residual HSQ and leave the devices air-clad. The fully etched waveguides had a width of 1 μm, and height of 1 μm (consisting of 650 nm of c-plane GaN and 350 nm of AlN buffer). The racetrack resonator devices have bend radii of 30 μm and straight sections of 65 μm. A microscope image of a GaN-on-sapphire racetrack resonator is shown in Fig. 2(a).

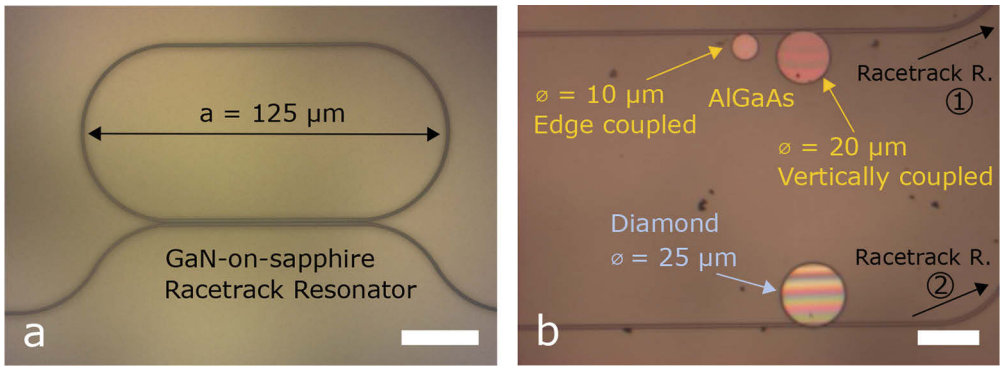

Fig. 2. (a) GaN-on-sapphire racetrack resonator. Scale bar = 20 μm. (b) Optical microscope image of 2 AlGaAs μ-disks and a diamond μ-disk resonator integrated onto the GaN-on-sapphire waveguide chip. Scale bar = 25 μm.

To print the μ-disk resonators, since their diameters are in the tens of μm range, μ-stamps were fabricated where the contact area of the PDMS pick-up element was of the same order of magnitude as the disks, as shown schematically in Fig. 1. The polymeric stamp was designed with a 50 μm vertical separation between the printing section and the remaining polymeric surface. This enables the capture and release of devices without the recessed PDMS surface interacting with neighboring devices.

2.2. Nanowire lasers

The serial integration of devices with critical dimension around 1 μm presents a more challenging situation. The second demonstration presented is the serial integration of NW lasers, where their long axes are aligned in parallel and the devices are spaced with a target separation of ~

Optical Materials EXPRESS

1 μm, as shown in Fig. 3. The NW lasers used in this work are bulk InP NW lasers [28] and core-shell GaAs/AlGaAs NWs [29], showing both room-temperature lasing emission in the wavelength ranges 840 - 900 nm and 700 - 800 nm, respectively. These NWs present hexagonal cross-sections but of different dimensions. Specifically, we used InP NW lasers of two different sizes, with average lengths of 5 and 10 μm and average diameters of 435 and 260 nm, respectively. The core/shell GaAs/AlGaAs NW lasers are of average diameters and lengths of $\sim$ 450 nm and $\sim$ 4 μm, respectively.

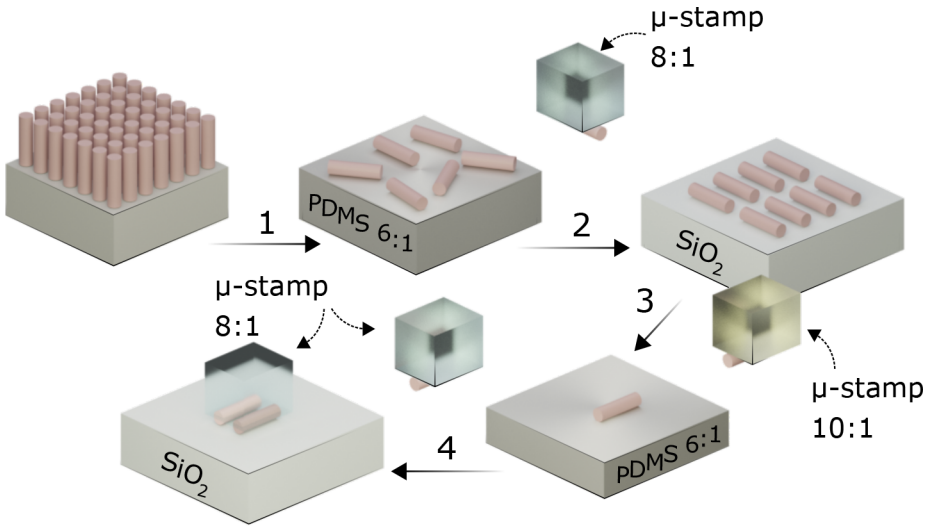

Fig. 3. The integration process of semiconductor NW devices from their growth substrate onto a receiving surface forming a laterally-aligned pair. (1) Direct contact with a 6:1 planar PDMS substrate produces a randomly distributed population of NWs. (2) An 8:1 PDMS stamp is used to select individual NWs and transfer them to a SiO_2 substrate for initial PL characterization. (3) Selected NWs are released from the SiO_2 substrate using a 10:1 PDMS stamp and transferred to an intermediate 6:1 PDMS substrate. (4) Serial printing of the NW's into spatially dense patterns is achieved using an 8:1 PDMS transfer stamp.

The sub-μm short axis dimension of the NW devices, and targeted μm scale spacing means that the PDMS stamp will be in contact with pre-printed devices during a subsequent printing step, as shown in Fig. 3, step 4. Therefore, a different strategy was developed compared with the μ-disk case. Here we use the material properties of the PDMS stamp, in addition to its geometry, to avoid re-adhesion or movement of pre-printed NWs during multiple, serial print steps. The printing cross-section of the PDMS stamps used in all processes detailed below presented a flat μ-tip with dimensions of 10×30 μm^2 [30].

The transfer printing process is fundamentally dependent on differential adhesion between the object to be printed and the PDMS stamp and the substrate. In general, the pick-up and deposition stages of transfer printing are differentiated by the velocity of the stamp removal [22]. In a serial printing process, where the stamp re-contacts an already printed device, the adhesion force between the in-situ device and the substrate must be greater than the force between the device and the stamp. The adhesive strength of PDMS can be controlled in its preparation through the ratio of the base to curing agents. Typically print stamps are prepared with a 10:1 ratio [30] that allows for reversible adhesion printing through velocity control. This formulation does allow for pick-up of already printed devices and so cannot be used for the serial NW printing process. Alternatively, a formulation with an 8:1 ratio cannot pick-up pre-printed devices from a SiO_2 receiver substrate. However, this also means that if a smooth intermediate substrate is used for

Optical Materials EXPRESS

the NW distribution step, an 8:1 ratio stamp will not be able to release these devices in order to print onto the final receiver substrate. The solution is to use a process where the intermediate substrate is less adhesive than the transfer stamp, which is in turn less adhesive than the final target receiver substrate.

In this work we use a multi-stage process with controlled competitive adhesion in each step to achieve controllable transfer of closely spaced NW devices, as shown in Fig. 3. First, the as-grown NW substrate is placed into direct contact with a 6:1 PDMS substrate which allows shearing of the devices and creates a randomly distributed population of NW's on the 6:1 PDMS substrate. Individual devices with similar long axis length are selected from that population and transferred to an intermediate SiO_2 substrate, using an 8:1 PDMS stamp, for optical characterization. The micro-photoluminescence (μ-PL) and optical spectrum measurements of the NW laser devices are carried out on a SiO_2 substrate to best match the conditions of the final receiver being targeted. After device selection, a 10:1 PDMS stamp is used to detach the NWs from the intermediate SiO_2 receiver and transfer them to a 6:1 PDMS substrate. The differential adhesion in favor of the 10:1 stamp requires that the NWs are laterally translated while in contact with the 6:1 PDMS receiver to allow their deposition. This step does not damage the NWs but has low spatial accuracy due to the lateral translation deposition required [30–32]. Finally, an 8:1 PDMS stamp is used to detach the NWs from the 6:1 PDMS substrate and serially transfer them onto the target SiO_2 receiver chip. The lasing characteristics of the NW devices were then re-measured where two closely spaced devices could be pumped with a single optical pump beam.

3. Results

3.1. Micro-disk resonators

To demonstrate the integration process using μ-disk resonators, we have printed two AlGaAs resonators and a diamond micro-disk resonator on two GaN-on-sapphire bus waveguides, all within a footprint of 50×120 μm^2, and with only 10 μm spacing between the 2 AlGaAs disks, as shown in Fig. 2(b). The GaN chip incorporated monolithic racetrack resonators that allowed measurement of the waveguide losses.

The waveguide spectra were measured using an end-fire transmission setup in the 1540 - 1600 nm band, with the transmission spectra pre- and post-printing of the AlGaAs and diamond disks shown in Figs. 4 and 5, respectively. An average loaded Q factor of 26,000 is measured over 37 resonances for the GaN racetrack resonators. A low distributed loss of 3.13 dB/cm is also measured, corresponding to a peak intrinsic Q factor of 122,000. The 10 and 20 μm diameter AlGaAs disks were printed with a separation of $\sim$ 10 μm onto a single GaN waveguide using the flexibility of the printing approach to demonstrate both edge coupling and vertical coupling between the disks and the bus waveguide. The transmission spectrum after printing exhibits additional resonances to the original GaN racetrack characteristics due to the coupling to the disks, as shown in Fig. 4. Average Q-factors of 14,000 and 7,600 for the edge and vertical coupled devices were measured, respectively. The resonances from each individual device were identifiable by free spectral range and an intermediate measurement after the first device was printed. An example resonance is shown in Fig. 4(d).

The 25 μm diameter diamond μ-disk was also transfer-printed onto the same chip, but targeting the adjacent GaN waveguide, as shown in Fig. 2. The measured Q-factor for the vertically coupled diamond μ-disk was found to be 91,000. As in previous work the transfer printing process does not induce additional losses in the resonators [27].

3.2. Nanowire lasers

To demonstrate that the technique does not induce any damage to the nanoscale integrated devices [32] and present an instance where sub-μm alignment proves to be useful for dense integration

Optical Materials EXPRESS

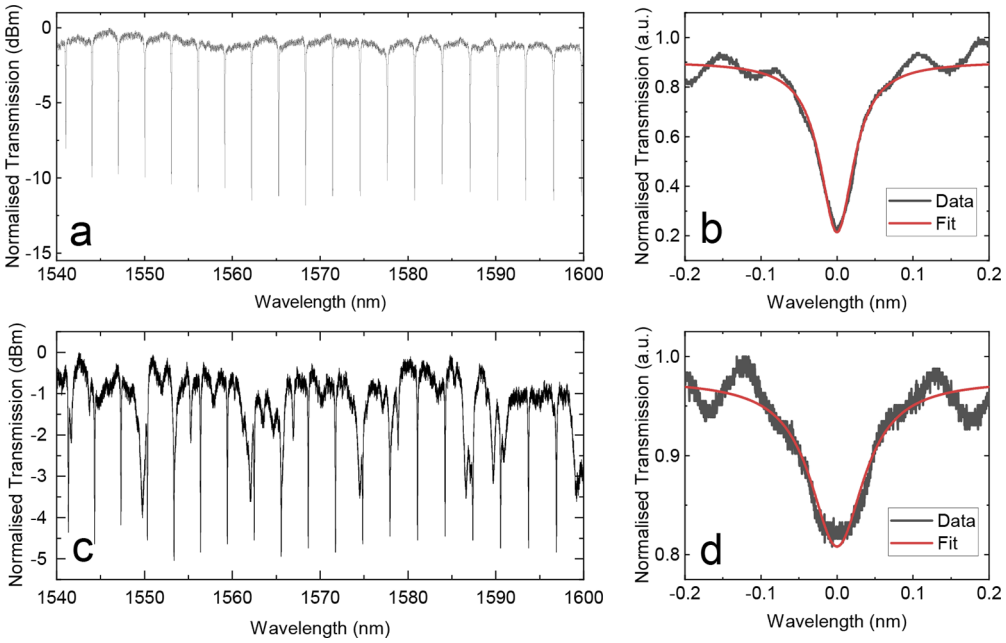

Fig. 4. (a) Transmission spectra of the corresponding GaN racetrack, with free spectral range ~ 3 nm. (b) Example fit of a resonance at 1558.8437 nm, FWHM = 53.6 pm, Q = 29,100. (c) Transmission spectra showing GaN (FSR 3 nm) and AlGaAs resonant lines for both (10 and 20 μm) μ-disks.

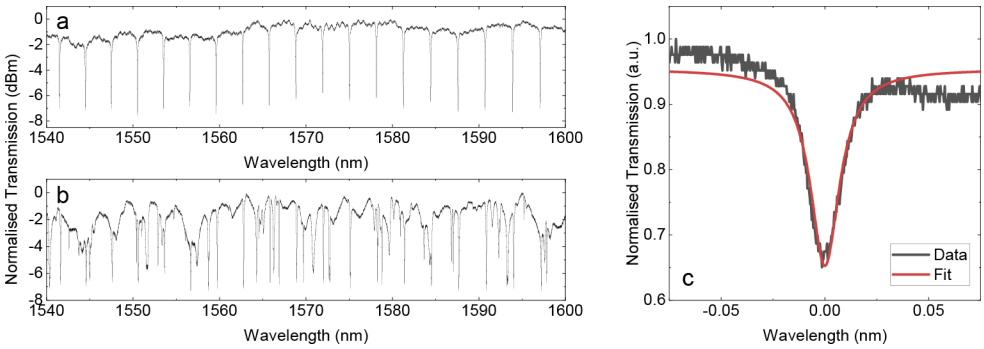

Fig. 5. (a) Transmission spectra of the corresponding GaN racetrack, with free spectral range ~ 3 nm. (b) Transmission spectra showing Diamond on GaN resonant lines. (c) Shows a resonance of a Diamond μ-disk with Q = 91,000.

of the devices on-chip, two sets of NW pairs were developed. In the first case, two NWs from the same material platform (InP) were used, with relatively similar lasing wavelength (~ 850 nm). A wider lasing wavelength span between two devices was then implemented using both GaAs/AlGaAs (~ 750 nm) and InP (~ 870 nm) devices in a single pair. As an initial stage, NWs from a single material source were deposited on a silica substrate and their wavelengths were measured using a μ-PL setup , as described in [30,31]. Results in Figs. 6(a-b) and 7(a-b) show characterization results for the single NW devices. Prior to the final integration and formation of nanolasers pairs, two devices were selected from the population based on their lasing wavelengths. These were then printed onto the intermediate adhesion PDMS substrate as

Optical Materials EXPRESS

detailed in the methods section before final printing onto a receiver silica substrate using the 8:1 ratio PDMS stamp. The final printing was carried out serially and the NWs were laterally aligned with target edge-to-edge separation of 1 μm. Due to the dimensions and structure of the NW laser pairs, these were optically excited at room temperature above their lasing threshold using a single pump beam with a spot size of ~ 1.6 μm (diameter). The two NWs were then re-measured in the μ-PL demonstrating the emission wavelengths of the pair to be compared with initial, separate measurements. Figures 6(c) and 7(c) show the lasing emission wavelengths for the InP-InP and GaAs/AlGaAs-InP NW pairs, respectively. The dark-field micrographs, in Figs. 6 and 7 show typical lasing emission pattern from the end-facets of the corresponding NW devices. Double spots are visible at the centres of the fringe patterns for the dual laser integration cases, showing the simultaneous lasing of the device pairs within the single pump spot. It is worth mentioning here, that the change in lasing emission wavelength in transfer-printed NW devices was investigated in [32].

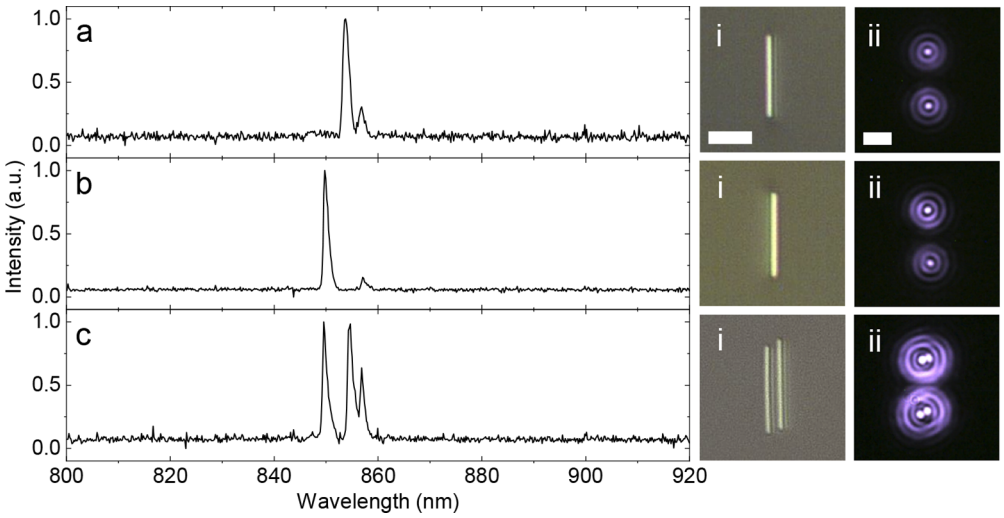

Fig. 6. (a and b) Room-temperature lasing spectra measured from two individually-operated InP NW lasers (diameter: 260 nm; length 10 μm) on a SiO_2 substrate. The insets plot dark- (i) and bright-field (ii) micrographs of the two InP NW lasers showing the achievement of lasing from the NWs' end-facets. (c) Room-temperature lasing spectra from the fabricated laterally-aligned NW laser system with fine wavelength spacing (< 10nm) between NWs. The insets show the fabricated NW laser system with closely spaced (1 μm side-to-side) laterally-aligned NW lasers and its emission under optical excitation. Scale bars = 5 μm.

Furthermore, we show that the positioning accuracy of the alignment procedure is comparable to that described in [24], even after serial contact print stages. Figure 8(a) shows SEM images of sets of InP NW laser pairs with varying target spatial separation, ranging between 1 – 3 μm. Due to the variability of NW lasers within a single growth batch, NWs of similar lengths were selected for printing using optical microscopy of the transfer-printing machine. The devices were then printed and laterally aligned onto a Si substrate using the aforementioned NW printing method. The alignment method to achieve a controlled lateral separation is reported in [24]. Four replicas of each target separation were fabricated. The separations were then assessed, using SEM images, as the centroid-to-centroid spacing of the NWs, and were within 188 nm (σ) of the targeted values. Figure 8(b) plots experimental results of the TP NW pairs of Si substrate against the target separations.

Optical Materials EXPRESS

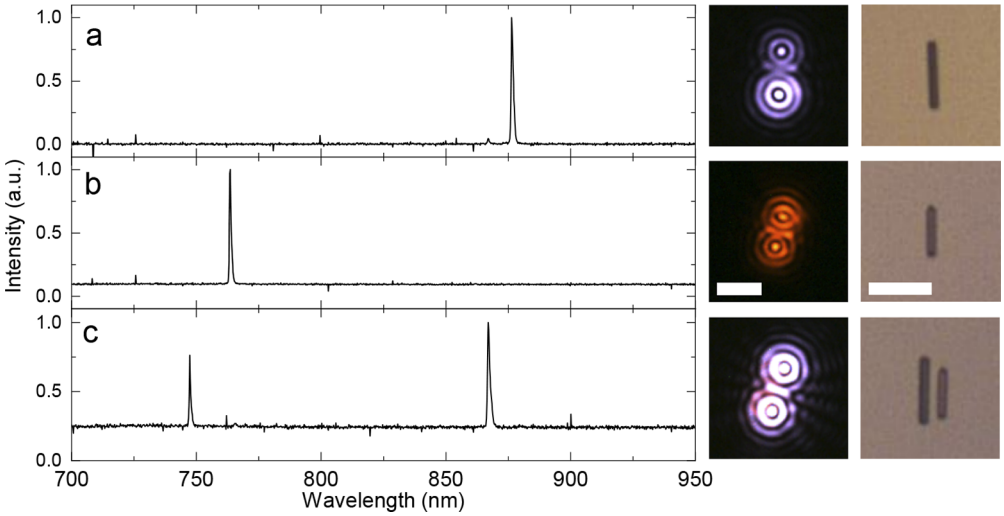

Fig. 7. Room-temperature lasing spectra of the individual (a) an InP NW and (b) core/shell GaAs/AlGaAs lasers on SiO_2 substrate. The insets plot dark- (i) and bright-field (ii) micrographs of the NW lasers showing the devices' structure and their lasing emission from the NWs end-facets. (c) Room-temperature lasing spectra from the fabricated coarse wavelength spacing (> 100 nm) NW. Scale bar = 5 μm.

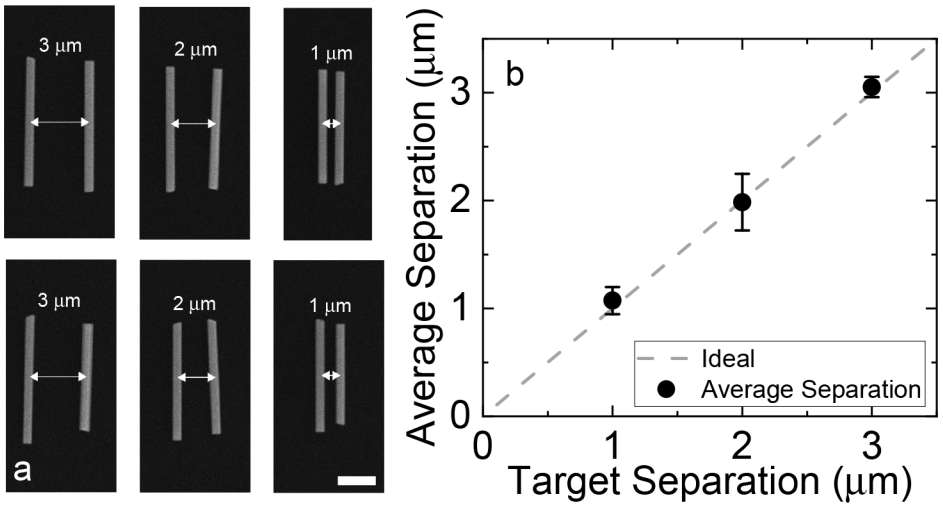

Fig. 8. (a) Representative SEM images of TP InP NW pair on Si substrate with target separations between the individual columns of 3, 2 and 1 μm, respectively. The values on the images show average lateral offset between the target and the calculated separations. Scale bar = 2 μm. (b) Scatter plot showing the difference between the calculated and target values for the printed InP NWs on Si.

Optical Materials EXPRESS

4. Conclusion

In this work we have presented transfer-printing methods that enable the integration of micro-/nano-photonic devices from multiple material sources with a footprint in order of the device size. The integration approaches were demonstrated using two distinctive micro-/nano-photonic devices: μ-disk resonators (diamond and AlGaAs) and NW lasers (core/shell GaAs/AlGaAs and bulk InP). Serial printing of the devices was enabled by the use of micron sized PDMS stamps and a multi-stage transfer process with tailored PDMS adhesion. The μ-disks were integrated onto a GaN-on-sapphire waveguide platform with existing monolithic racetrack resonators. The combined system demonstrated the integration of three different materials within a footprint of $\sim 50 \times 120\ \mu m^2$. The transfer-printed NW pairs were fabricated with control over device to device spacing in the hundreds of nanometers regime and showed controlled lasing emission in targeted wavelength regions when optically excited with a single pump beam (spot size, d $\sim$ 1.6 μm). These techniques represent an important advance for the integration of multiple materials onto a single PIC chip system without requiring the host PICs to withstand post-processing stages of lithography and etching. Furthermore, integration of planar membrane waveguide and nanowire devices can be envisaged in future hybrid systems on a single chip. These integration routes are also fully compatible with the previously reported sub-μm alignment techniques [24], making the transfer printing a versatile and back-end compatible integration technique.

Funding. Engineering and Physical Sciences Research Council (EP/R03480X/1, EP/P013597/1, EP/P013570/1); European Commission (Grant No. 828841 ChipAI-H2020-FETOPEN-2018–2020, Grant No. 829116 SuperPixels-H2020-FETOPEN-2018-2020); Royal Academy of Engineering under the Research Chairs and Senior Research fellowships scheme; Fraunhofer UK.

Disclosures. The authors declare no conflicts of interest.

Data Availability. The data that support the findings of this study are openly available in the University of Strathclyde's KnowledgeBase, Ref. [33]

References

1. W. Bogaerts, D. Taillaert, B. Luyssaert, P. Dumon, J. V. Campenhout, P. Bienstman, D. V. Thourhout, R. Baets, V. Wiaux, and S. Beckx, "Basic structures for photonic integrated circuits in silicon-on-insulator," Opt. Express **12**(8), 1583 (2004).
2. T. Koch and U. Koren, "Semiconductor photonic integrated circuits," IEEE J. Quantum Electron. **27**(3), 641–653 (1991).
3. S. Y. Siew, B. Li, F. Gao, H. Y. Zheng, W. Zhang, P. Guo, S. W. Xie, A. Song, B. Dong, L. W. Luo, C. Li, X. Luo, and P. G.-Q. Lo, "Review of silicon photonics technology and platform development," Journal of Lightwave Technology **13**, 4374–4389 (2021).
4. M. Smit, K. Williams, and J. van der Tol, "Past, present, and future of InP-based photonic integration," APL Photonics **4**(5), 050901 (2019).
5. H. Wong, V. Filip, C. Wong, and P. Chung, "Silicon integrated photonics begins to revolutionize," Microelectron. Reliab. **47**(1), 1–10 (2007).
6. X. Zou, F. Zou, Z. Cao, B. Lu, X. Yan, G. Yu, X. Deng, B. Luo, L. Yan, W. Pan, J. Yao, and A. M. J. Koonen, "A multifunctional photonic integrated circuit for diverse microwave signal generation, transmission, and processing," Laser Photonics Rev. **13**(6), 1800240 (2019).
7. T. Sharma, J. Wang, B. K. Kaushik, Z. Cheng, R. Kumar, Z. Wei, and X. Li, "Review of recent progress on silicon nitride-based photonic integrated circuits," IEEE Access **8**, 195436–195446 (2020).
8. I. Prieto, J. Herranz, L. Wewior, Y. González, B. Alén, L. González, and P. A. Postigo, "High quality factor GaAs-based photonic crystal microcavities by epitaxial re-growth," Opt. Express **21**(25), 31615 (2013).
9. G.-H. Duan, C. Jany, A. L. Liepvre, A. Accard, M. Lamponi, D. Make, P. Kaspar, G. Levaufre, N. Girard, F. Lelarge, J.-M. Fedeli, A. Descos, B. B. Bakir, S. Messaoudene, D. Bordel, S. Menezo, G. de Valicourt, S. Keyvaninia, G. Roelkens, D. V. Thourhout, D. J. Thomson, F. Y. Gardes, and G. T. Reed, "Hybrid III–v on silicon lasers for photonic integrated circuits on silicon," IEEE J. Sel. Top. Quantum Electron. **20**(4), 158–170 (2014).
10. J.-H. Kim, S. Aghaeimeibodi, J. Carolan, D. Englund, and E. Waks, "Hybrid integration methods for on-chip quantum photonics," Optica **7**(4), 291 (2020).
11. A. W. Elshaari, A. Skalli, S. Gyger, M. Nurizzo, L. Schweickert, I. E. Zadeh, M. Svedendahl, S. Steinhauer, and V. Zwiller, "Deterministic integration of hBN emitter in silicon nitride photonic waveguide," Adv. Quantum Technol. **4**(6), 2100032 (2021).

Optical Materials EXPRESS

12. G. Roelkens, J. V. Campenhout, J. Brouckaert, D. V. Thourhout, R. Baets, P. R. Romeo, P. Regreny, A. Kazmierczak, C. Seassal, X. Letartre, G. Hollinger, J. Fedeli, L. D. Cioccio, and C. Lagahe-Blanchard, "III-v/si photonics by die-to-wafer bonding," Mater. Today **10**(7-8), 36–43 (2007).
13. Q. Li and K. M. Lau, "Epitaxial growth of highly mismatched III-v materials on (001) silicon for electronics and optoelectronics," Prog. Cryst. Growth Charact. Mater. **63**(4), 105–120 (2017).
14. H. Kim, W.-J. Lee, A. C. Farrell, J. S. D. Morales, P. Senanayake, S. V. Prikhodko, T. J. Ochalski, and D. L. Huffaker, "Monolithic InGaAs nanowire array lasers on silicon-on-insulator operating at room temperature," Nano Lett. **17**(6), 3465–3470 (2017).
15. G. Koblmüller, B. Mayer, T. Stettner, G. Abstreiter, and J. J. Finley, "GaAs–AlGaAs core–shell nanowire lasers on silicon: invited review," Semicond. Sci. Technol. **32**(5), 053001 (2017).
16. S. Mauthe, H. Schmid, K. E. Moselund, N. V. Trivino, M. Sousa, P. Staudinger, Y. Baumgartner, P. Tiwari, T. Stoferle, D. Caimi, and M. Scherrer, "Monolithic integration of III-v microdisk lasers on silicon," in *2019 International Conference on Optical MEMS and Nanophotonics (OMN)*, (IEEE, 2019).
17. J. McPhillimy, B. Guilhabert, C. Klitis, M. D. Dawson, M. Sorel, and M. J. Strain, "High accuracy transfer printing of single-mode membrane silicon photonic devices," Opt. Express **26**(13), 16679 (2018).
18. J. Zhang, G. Muliuk, J. Juvert, S. Kumari, J. Goyvaerts, B. Haq, C. O. de Beeck, B. Kuyken, G. Morthier, D. V. Thourhout, R. Baets, G. Lepage, P. Verheyen, J. V. Campenhout, A. Gocalinska, J. O'Callaghan, E. Pelucchi, K. Thomas, B. Corbett, A. J. Trindade, and G. Roelkens, "III-v-on-si photonic integrated circuits realized using micro-transfer-printing," APL Photonics **4**(11), 110803 (2019).
19. H. Yang, D. Zhao, S. Chuwongin, J.-H. Seo, W. Yang, Y. Shuai, J. Berggren, M. Hammar, Z. Ma, and W. Zhou, "Transfer-printed stacked nanomembrane lasers on silicon," Nat. Photonics **6**(9), 615–620 (2012).
20. B. Corbett, R. Loi, W. Zhou, D. Liu, and Z. Ma, "Transfer print techniques for heterogeneous integration of photonic components," Prog. Quantum Electron. **52**, 1–17 (2017).
21. H. Kum, D. Lee, W. Kong, H. Kim, Y. Park, Y. Kim, Y. Baek, S.-H. Bae, K. Lee, and J. Kim, "Epitaxial growth and layer-transfer techniques for heterogeneous integration of materials for electronic and photonic devices," Nat. Electron. **2**(10), 439–450 (2019).
22. A. Carlson, A. M. Bowen, Y. Huang, R. G. Nuzzo, and J. A. Rogers, "Transfer printing techniques for materials assembly and micro/nanodevice fabrication," Adv. Mater. **24**(39), 5284–5318 (2012).
23. J. Zhang, B. Haq, J. O'Callaghan, A. Gocalinska, E. Pelucchi, A. J. Trindade, B. Corbett, G. Morthier, and G. Roelkens, "Transfer-printing-based integration of a III-v-on-silicon distributed feedback laser," Opt. Express **26**(7), 8821 (2018).
24. J. McPhillimy, D. Jevtics, B. J. E. Guilhabert, C. Klitis, A. Hurtado, M. Sorel, M. D. Dawson, and M. J. Strain, "Automated nanoscale absolute accuracy alignment system for transfer printing," ACS Appl. Nano Mater. **3**(10), 10326–10332 (2020).
25. B. Guilhabert, J. McPhillimy, S. May, C. Klitis, M. D. Dawson, M. Sorel, and M. J. Strain, "Hybrid integration of an evanescently coupled AlGaAs microdisk resonator with a silicon waveguide by nanoscale-accuracy transfer printing," Opt. Lett. **43**(20), 4883 (2018).
26. P. Hill, C. Klitis, B. Guilhabert, M. Sorel, E. Gu, M. D. Dawson, and M. J. Strain, "All-optical tuning of a diamond micro-disk resonator on silicon," Photonics Res. **8**(3), 318 (2020).
27. J. McPhillimy, S. May, C. Klitis, B. Guilhabert, M. D. Dawson, M. Sorel, and M. J. Strain, "Transfer printing of AlGaAs-on-SOI microdisk resonators for selective mode coupling and low-power nonlinear processes," Opt. Lett. **45**(4), 881 (2020).
28. Q. Gao, D. Saxena, F. Wang, L. Fu, S. Mokkapati, Y. Guo, L. Li, J. Wong-Leung, P. Caroff, H. H. Tan, and C. Jagadish, "Selective-area epitaxy of pure wurtzite InP nanowires: High quantum efficiency and room-temperature lasing," Nano Lett. **14**(9), 5206–5211 (2014).
29. D. Saxena, N. Jiang, X. Yuan, S. Mokkapati, Y. Guo, H. H. Tan, and C. Jagadish, "Design and room-temperature operation of GaAs/AlGaAs multiple quantum well nanowire lasers," Nano Lett. **16**(8), 5080–5086 (2016).
30. B. Guilhabert, A. Hurtado, D. Jevtics, Q. Gao, H. H. Tan, C. Jagadish, and M. D. Dawson, "Transfer printing of semiconductor nanowires with lasing emission for controllable nanophotonic device fabrication," ACS Nano **10**(4), 3951–3958 (2016).
31. D. Jevtics, A. Hurtado, B. Guilhabert, J. McPhillimy, G. Cantarella, Q. Gao, H. H. Tan, C. Jagadish, M. J. Strain, and M. D. Dawson, "Integration of semiconductor nanowire lasers with polymeric waveguide devices on a mechanically flexible substrate," Nano Lett. **17**(10), 5990–5994 (2017).
32. D. Jevtics, J. McPhillimy, B. Guilhabert, J. A. Alanis, H. H. Tan, C. Jagadish, M. D. Dawson, A. Hurtado, P. Parkinson, and M. J. Strain, "Characterization, selection, and microassembly of nanowire laser systems," Nano Lett. **20**(3), 1862–1868 (2020).
33. D. Jevtics, J. A. Smith, J. McPhillimy, B. Guilhabert, P. Hill, C. Klitis, A. Hurtado, M. Sorel, H. H. Tan, C. Jagadish, M. D. Dawson, and M. J. Strain, "Data for: spatially dense integration of micron-scale devices from multiple materials on a single chip via transfer-printing," University of Strathclyde, KnowledgeBase, Dataset, 2021, https://doi.org/10.15129/10070904-bb8a-433c-875d-cdd5e6bcda95.